

Molecular Template Approach for Evolution of Conducting Polymer Nanostructures: Tracing the Role of Morphology on Conductivity and Solid State Ordering

M. Jinish Antony[†] and M. Jayakannan^{*,‡}

Chemical Sciences and Technology Division, National Institute for Interdisciplinary Science and Technology, Thiruvananthapuram 695019, Kerala, India, and Department of Chemistry, Indian Institute of Science Education and Research (IISER), 900, NCL Innovation Park, Dr. Homi Bhabha Road, Pune—411 008, Maharashtra, India

Received: November 8, 2009; Revised Manuscript Received: December 2, 2009

Here, we report a unique molecular template approach, for the first time, to study the evolution of the different types of nanomaterial morphologies such as nanofiber, nanorod, nanosphere, and nanotube in a single system without changing their chemical composition or polymerization route. A renewable resource surfactant was self-organized with aniline (95%) and pyrrole (5%) in water to produce white emulsion consisting of long-range cylindrical micellar aggregates. The dilution of the emulsion with water resulted in the transformation of cylindrical to vesicular aggregates without any phase separation. The size and shape of the cylindrical and vesicular template aggregates were confirmed by dynamic light scattering and electron microscopic analysis. The chemical oxidation of the cylindrical templates produced nanofibers and nanorods, whereas hollow spheres and nanotubes were produced by vesicular templates. The nanofibers were found as long as 4–5 μm length with 200 nm widths, whereas the nanorods were shorter in length (0.5–0.7 μm) with 80–120 nm diameter. The hollow spheres were obtained in 1 μm diameter with wall thickness of ~80 nm. The length of the nanotubes was found to vary from 1.2 to 1.8 μm . The average wall thickness and inner pore diameter of the nanotubes were found as ~30 nm and ~60 nm, respectively. The size and shape of the template aggregates match very well with that of the synthesized nanomaterials and provide direct evidence for the template-assisted evolution of the nanostructure morphology. NMR, FT-IR and UV-visible spectroscopies were utilized to confirm the structure and electronic properties of the nanomaterials. Wide angle X-ray diffraction and transmission electron microscopy—electron diffraction analysis revealed that the nanotubes possessed three-dimensional lamellar-type solid states ordering with high percent crystallinity up to 60%. Variable temperature four-probe conductivity measurements of all samples showed typical I – V plots. The conductivity of the nanofibers was found one order higher than that of nanorod, hollow sphere, and nanotubes at all temperatures. The present investigation enabled us to establish the role of various types of nanomorphologies on properties of nanomaterials such as conductivity and solid state ordering without change in their chemical composition.

Introduction

One and three-dimensional conducting polymer nanomaterials have found numerous applications in electronic, electrochemical, mechanical, and biological fields.^{1–10} Shape and size of these nanomaterials were found very crucial for their functioning in electronic devices and delivery applications.^{11,12} Among the various conducting nanomaterials, polythiophene, polyaniline and polypyrrole are important classes of conducting polymers having the advantage of excellent environmental and chemical stability.¹³ Micellar self-assemblies of both cationic and anionic surfactants were demonstrated as useful templates for the synthesis of conducting nanomaterials.^{13–20} However, there is a large inconsistency over the choice of these surfactants for templating conducting polymer nanostructures. For example, cationic surfactants like cetyltrimethylammonium bromide and dodecyltrimethylammonium bromide were found to template successfully for polypyrrole nanofibers, whereas they were found not suitable for polyaniline nanomaterials.^{13–16} On the other hand, anionic surfactants of sulfonic acid derivatives were found

to be more suitable templates for polyaniline nanofibers and inefficient for polypyrroles.¹⁷ Anionic surfactants have additional advantages that they could behave both as template surfactant as well as negatively charged anionic counterpart for stabilizing the positively charged conducting polymer chains.^{17–22} The morphology of polypyrrole and polyaniline were found almost intrinsic to their polymer structures; the polymerization of aniline and pyrrole exclusively produce nanofibers and nanospheres, respectively. Few attempts were reported in literature to bridge the gap between these two important conducting polymers by the way of making their copolymer derivatives.^{23–29} The copolymer nanomaterials are unique and important because they possess mixed properties which are not available in either of their homopolymers. However, the limitation in the choice of the surfactant molecules which could template simultaneously for both aniline and pyrrole monomers hampered the study of the role of morphology on the nanomaterial properties. Recently, we have developed new amphiphilic surfactant molecules from renewable resource starting materials for polyaniline nanofibers.³⁰ Various polymerization techniques such as emulsion, interfacial, and dispersion were employed to tune the shapes of polyaniline nanomaterials like nanospheres and nanofibers.³⁰ In our effort to develop surfactant-mediated approach for poly-

* To whom correspondence should be addressed. E-mail: jayakannan@iiserpune.ac.in. Fax: 0091-20-25898022.

[†] National Institute for Interdisciplinary Science and Technology.

[‡] Indian Institute of Science Education and Research (IISER).

pyrrole, the renewable resource azobenzenesulfonic acid derivative was utilized to precisely control the size of the polypyrrole nanospheres from 50 to 500 nm.³¹ The renewable dopant-cum-surfactant designed by us could be utilized for both aniline and pyrrole monomers under identical emulsion polymerization conditions. The preliminary investigation on the copolymerization of aniline and pyrrole using the above surfactant revealed that composition of the monomers played a significant role in determining the morphology of the nanomaterials.^{31b} Thus, our custom designed surfactant provides new opportunities in conducting nanomaterials for tracing the phenomena of evolution of nanomorphologies in a polyaniline-*co*-polypyrrole system. The approach was aimed to address the following important unanswered questions in conducting polymer nanomaterials: (i) The evolution of the different types of morphologies such as nanofiber, nanorod, nanosphere, and nanotube were obtained in a single polymerization medium without changing their chemical composition or polymerization routes. (ii) To attain the above objective, a dilute polymerization technique was developed for the fixed composition of the surfactant, aniline, and pyrrole that varies the concentration of the reaction chemical constituents by diluting with water. (iii) The role of the various nanomorphologies on properties such as conductivity, solid state ordering, percent crystallinity, and electronic features were established, and (iv) variable temperature *I*–*V* techniques were utilized to study the role of the morphology on the solid state conductivity.

The present investigation emphasizes the evolution of nanomaterials morphologies in polyaniline–polypyrrole copolymers (like nanofiber-to-nanorod-to-hollow sphere-to-nanotube) via self-assembled molecular templates. A custom designed renewable amphiphilic azobenzenesulfonic acid dopant was reacted with aniline and pyrrole in water to produce a thick emulsion. The chemical compositions of [aniline]:[pyrrole] and [monomers]/[dopant] were fixed, and the concentration was varied by diluting with various amounts of water to fine tune the morphological transformation. The templates were subjected to chemical oxidation using ammonium persulfate to produce copolymer nanomaterials. Electron microscopic analysis of samples revealed that the conducting polymer morphologies undergo transformation from nanofibers to nanorods and further extended to hollow spheres to well-defined nanotubes. Dynamic light scattering and scanning electron microscopy analysis of the polymerization mixtures revealed that the templates underwent transformation from cylindrical to vesicular aggregates, which account for morphological transformation in the nanomaterials. Further, these nanomaterials were submitted to absorption, NMR, FT-IR, temperature-dependent four-probe conductivity measurements, and wide-angle X-ray diffraction (WXRD) analysis to study the structure property relationship and establish the correlation between the morphology with solid state conductivity. The detailed investigation revealed that the conducting polymer nanofiber morphology was found to show superior conductivity behaviors compared to all other nanostructures such as nanorod, hollow sphere, and nanotube for identical chemical composition under same polymerization route.

Experimental Section

Materials. Pyrrole, aniline, ammoniumpersulfate (APS), and sulfanilic acid were purchased from Aldrich Chemicals. Cardanol was purified by double-vacuum distillation at 3–4 mm of Hg, and the fraction distilled at 220–235 °C was collected. The amphiphilic dopant 4-[4-hydroxy-2((Z)-pentadec-8-enyl)

phenylazo]-benzenesulfonic acid was synthesized from cardanol as reported earlier.³¹

Measurements. ¹H NMR analysis of the dopant and polymer samples were carried out in 500-MHz Bruker Avance ii NMR spectrometer in *d*₆-dimethyl sulfoxide (DMSO) containing a small amount of tetramethylsilane (TMS) as internal standard. Infrared spectra of the polymers were recorded using Perkin-Elmer Spectrum 1 FT-IR spectrometer in the range of 4000–400 cm^{−1}. The purity of the compounds was determined by fast atom bombardment high-resolution mass spectrometry (FAB-HRMS: JEOL JSM 600). For conductivity measurements, the polymer samples were pressed into a 10 mm diameter and 1 mm thickness pellet and analyzed using a four-probe Keithley 6221 DC and AC current source and 2181A nanovoltmeter. The temperature-dependent conductivity of the sample is measured with the help of PID controlled heating oven. For SEM measurements, polymer samples were subjected to a thin gold coating using a JEOL JFC-1200 fine coater. The probing side was inserted into a JEOL JSM-5600 LV scanning electron microscope for taking photographs. WXRD patterns of the finely powdered polymer samples were recorded by a Philips analytical diffractometer using Cu K α emission. The spectra were recorded in the range of 2 θ = 0–40 and analyzed using X'Pert software. UV–visible spectra of the copolymers are recorded using a Perkin-Elmer Lambda-35 UV–visible spectrometer. TEM analysis was recorded using a Tecnai 30 G² S-twin 300 KV high resolution transmission electron microscope. For TEM measurements a suspension of nanomaterials was prepared in ethanol and deposited on a Formvar-coated copper grid. DLS measurement was done by Nano ZS Malvern instrument employing a 4 mW He–Ne laser (λ = 632.8 nm), equipped with a thermostated sample chamber. The thermal stability of the polymers was determined using PerkinElmer STA 6000 simultaneous thermal analyzer at a heating rate of 10 °C/min in nitrogen. The TGA instrument was calibrated with calcium oxalate monohydrate as standard.

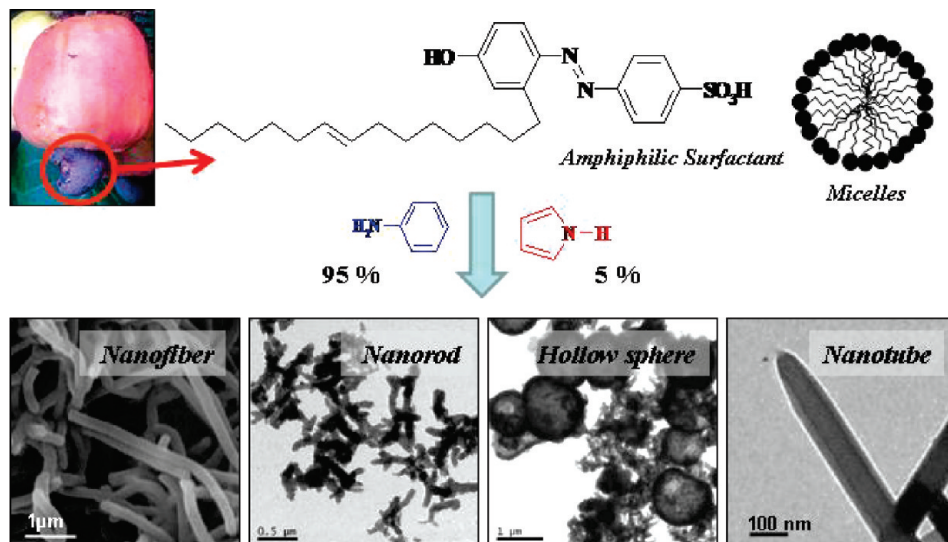
Preparation of Polyaniline Nanofiber via Emulsion Route. Surfactant 1 (70 mg, 0.144 mmol) was taken in 10 mL of water and stirred under sonication for 15 min. Aniline (1 mL, 11 mmol) was added to the surfactant solution, and the mixture was sonicated for 45 min. At the end of stirring, the polymerization mixture turned into a pale yellow thick emulsion. Ammonium persulfate (3.28 g, 14.4 mmol) in water (5 mL) was added dropwise to the solution, and the stirring continued under sonication for 1 h. The polymerization was continued without disturbance for 12 h at 25 °C. The sample was filtered and washed with water and methanol until the filtrate became colorless. The green nanomaterial was dried in a vacuum oven for 12 h at 50 °C. Yield = 87%. ¹H NMR (*d*₆-DMSO) δ : 7.40 (m, 2H, PANI), 7.44 (m, 2H, PANI), 7.78 (s, 4H, Ar–H dopant). FT-IR (KBr, cm^{−1}): 1560, 1494, 1346, 1193, 1111, 1050, 923, 811, 783, and 612. UV–vis (in water): 350, 450, and 900 nm.

Preparation of Polyaniline-*co*-polypyrrole Nanomaterials via Dilution Route. Typical procedure for the synthesis of P-Co-5 is given below. Surfactant 1 (70 mg, 0.144 mmol) was taken in 10 mL of water and stirred under sonication for 15 min. Pyrrole (0.05 mL, 0.72 mmol) and aniline (0.95 mL, 10.5 mmol) were added to the surfactant solution, and the mixture was sonicated for 45 min. At the end of stirring, the polymerization mixture turned into a pale yellow thick emulsion. Ammonium per sulfate (3.28 g, 14.4 mmol) in water (5 mL) was added dropwise to the solution, and stirring was continued under sonication for 1 h. The polymerization was continued without disturbance for 12 h at 25 °C. The sample was filtered

TABLE 1: Concentration of Reactants, Elemental Analysis, and Degradation Temperature

sample ^a	concen of aniline (M)	concn of pyrrole (M)	concn of surfactant (M)	amount of water (mL) ^b	S/N ratio ^c	TGA ^d (°C)	η_{inh}^e (dL/g)
PANI	7.3×10^{-1}	—	9.6×10^{-3}	10	0.43	270	0.28
P-Co-5	7.0×10^{-1}	4.8×10^{-2}	9.6×10^{-3}	10	0.41	270	0.24
P-20	4.2×10^{-1}	2.9×10^{-2}	5.8×10^{-3}	20	0.40	270	0.24
P-50	1.9×10^{-1}	1.3×10^{-2}	2.6×10^{-3}	50	0.40	270	0.27
P-100	1.0×10^{-1}	6.9×10^{-3}	1.4×10^{-3}	100	0.35	270	0.28

^a PANI represent the homopolymer and P-Co-5, P-20, P-50, P-100 are copolymers. ^b Ammonium persulfate (14.4 mmol) in 5 mL of water was added into the polymerization mixture containing different amounts of water. ^c Obtained from elemental analysis. ^d The degree of decomposition for 10% decomposition. ^e The inherent viscosity of polymer solution (0.5 wt %) is measured in NMP at 25 °C.

**Figure 1.** Schematic representation of the synthesis of nanomaterials.

and washed with water and methanol until the filtrate become colorless. The copolymer nanomaterial was dried in a vacuum oven for 12 h at 50 °C. Yield = 75%. ¹H NMR (*d*₆-DMSO) δ: 7.40 (m, 2H, PANI), 7.44 (m, 2H, PANI), 7.29 (d, 2H, PPy), 7.78 (s, 4H, dopant). FT-IR (KBr, cm⁻¹): 1560, 1494, 1346, 1193, 1111, 1050, 923, 811, 783, and 612. UV-vis (water): 350, 450, and 900 nm.

Polymer P-20, P-50 and P-100 were synthesized using the above procedure by diluting the polymerization mixture with various amount of water. The concentration of the reactants, amount of water, elemental analysis and TGA data are provided in table 1.

Results and Discussion

Amphiphilic water-soluble anionic surfactant 4-[4-hydroxy-2(Z)-pentadec-8-enyl]phenylazo]benzenesulfonic acid was synthesized from naturally occurring cardanol, which is a pollutant from the cashew nut processing industry (see Figure 1). The structure of the azobenzenesulfonic acid was confirmed by NMR, FT-IR, and mass (see Supporting Information). The surfactant has a unique built-in amphiphilic design in which the hydrophilic sulfonic acid behaves as a polar head and the long alkyl chain as a hydrophobic tail. The renewable anionic amphiphilic surfactant exists as 4.3 nm micelles in water and the critical micelle concentration (CMC) was determined as 6×10^{-4} M.^{30d} Emulsion polymerization of the amphiphilic dopant micelles with monomers like aniline and pyrrole produced their corresponding nanofibers and nanospheres, respectively.^{30,31} The size and shape of these nanomaterials were unaltered for a wide range of [monomer]/[dopant] concentration and also less susceptible to variation in the experimental conditions such as ultrasonic stirring, temperature, etc.^{30,31} In

the present investigation, the dopant micelles were utilized for evolution of nanomaterial morphology ranging from nanofibers, nanorods, and hollow spheres to nanotubes via aniline + pyrrole copolymerization approach (see Figure 1). The compositions of reaction constituents were fixed, while concentrations were systematically varied by diluting the thick emulsion by a known amount of water. The chemical compositions of [aniline]:[pyrrole] and [monomers]/[dopant] were fixed as 95:5 and 75, respectively, on the basis of previous experience.^{31b} The systematic variation of the pyrrole and aniline composition in our earlier attempt^{31b} revealed that transformation of morphology from fiber to rod to sphere predominantly occurred for less than 10% pyrrole in the feed. On the basis of this knowledge, in the present investigation the composition of pyrrole was restricted up to 5 mol % in the feed. The exact concentration of the reaction constituents and amount of water utilized in the dilute polymerization route was summarized in Table 1. The polymerization mixtures consisted of the same composition of aniline, pyrrole, and surfactants but largely varied by their concentration in water. The concentration of the amphiphilic dopant was maintained always higher than its CMC to retain its micellar behavior in water. This had facilitated the stabilization of the aromatic monomers (aniline and pyrrole) without phase separation even at large dilution (at 100 mL). Pyrrole composition was fixed as 5 mol % in the feed because of two reasons: (i) the morphology transformation was predominant at lower composition of pyrrole in the feed and (ii) at higher incorporation of pyrrole, the copolymers were found insoluble which restrict their structural characterization by NMR.^{31a} The emulsions were found to be very stable for more than a week at ambient conditions. These polymerization mixtures were oxidized by adding aqueous solutions of ammonium persulfate in

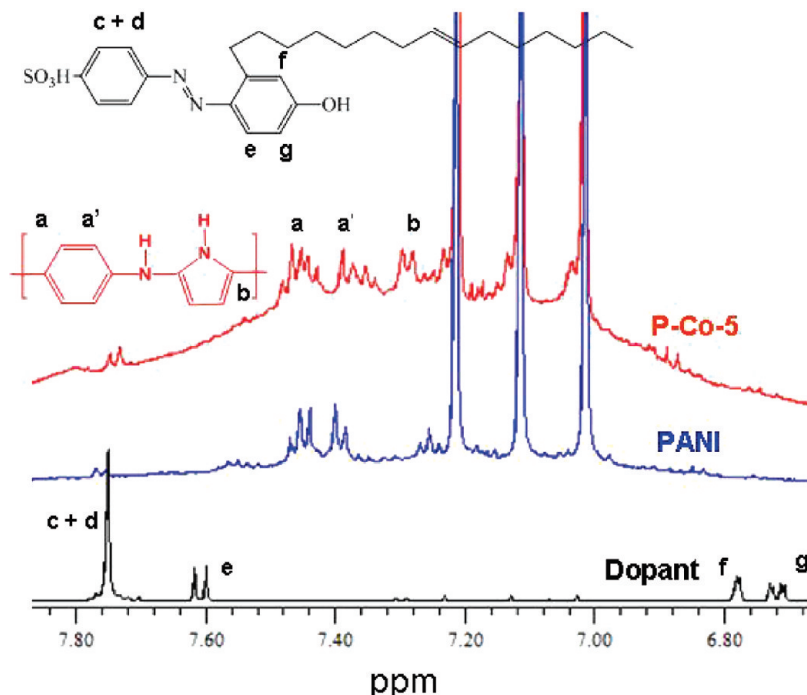


Figure 2. ^1H NMR spectra of surfactant, **PANI**, and **P-Co-5** in d_6 -DMSO.

ice cold conditions and keeping the reaction mixture without any disturbance for overnight. The resultant dark green material was filtered and washed with water and methanol until the filtrate became colorless. It was dried under vacuum oven for 24 h (0.05 mm of Hg) at 50 °C prior to further analysis. The copolymers are represented by **P-Co-5**, **P-20**, **P-50**, and **P-100**. The number in **P-Co-5** represents 5 mol % pyrrole feed, which is synthesized in 10 mL of water, while the others, **P-20**, **P-50**, and **P-100**, represent the amount of water (20, 50, and 100 mL) added for the dilution. Polyaniline nanofiber (**PANI**) was synthesized by polymerizing the thick emulsion of aniline with dopant (no pyrrole monomer) under identical conditions.

The structures of the copolymer nanomaterials were characterized by ^1H NMR and FT-IR. Typically polyaniline nanomaterials are insoluble in nature, interestingly the amphiphilic dopant enhances the solubility of the nanomaterials for structural characterization. The NMR spectra of dopant, **PANI**, and **P-Co-5** were recorded in d_6 -DMSO and were shown in Figure 2. The dopant showed peaks at 7.78, 7.60, 6.77, and 6.71 ppm corresponding to different types of aromatic protons. **PANI** contains two sets of aromatic protons at 7.45 and 7.40 ppm.^{32,33} Copolymer **P-Co-5** showed a peak at 7.29 ppm corresponding to β -protons in pyrrole.^{31,34–36} The comparison of the integral intensities of polyaniline with β -protons of pyrrole revealed 16 mol % incorporation of pyrrole in the copolymer. A similar composition determination for the other dilute polymerization samples **P-20** and **P-50** confirmed the pyrrole content in the range of 16–18% (see Supporting Information). **P-100** was found insoluble in d_6 -DMSO and its NMR spectrum was not good. The high incorporation of pyrrole in the copolymer was correlated to the high reactivity ratio of pyrrole ($r_{\text{PY}} = 2.16$) over aniline in oxidative polymerization route.²⁷ NMR spectra analysis confirmed the incorporation of ~16 to 18% pyrrole in the copolymer for the 5% of the pyrrole monomer in the feed. It suggests that the pyrrole monomer possessed reactivity almost 3 times higher than that of aniline, which almost matched with the earlier reports. However, a detail copolymerization kinetics of the aniline and pyrrole is required to determine their reactivity

ratios. FT-IR spectra of the copolymers were recorded in KBr (see Supporting Information). The polyaniline sample **PANI** has two peaks at 1580 and 1490 cm^{-1} with respect to stretching vibration of quinoid and benzenoid in polyaniline chains, respectively.^{30,37} Three additional peaks were assigned at 1300, 1148, and 820 cm^{-1} to C–N stretching of secondary amine group, O=S=O stretching of the sulfonic acid dopant, and C–H out-of-plane stretching in the 1,4-disubstituted benzene ring, respectively.^{31,38–40} Copolymers formation is indicated by in-plane deformation of (N–H or C–H) at 1047 cm^{-1} which increases the intensity from **PANI** to **P-Co-5**, **P-20**, **P-50**, **P-100**, respectively. Thermal stability of the nanomaterials were determined by TGA and thermograms are provided as Supporting Information. The copolymer nanomaterials had high thermal stability, and only 10% weight loss was observed at temperatures lower than 280 °C. This indicated that the azobenzenesulfonic acid doped nanomaterials were thermally stable as reported for other dopants such as camphorsulfonic acid.²²

The morphology of the nanomaterials was recorded using JEOL JSM-5600 LV scanning electron microscope (SEM) and images are shown in Figure 3. The morphology of **PANI** showed a mat of thick and long nanofibers of length up to 4–6 μm and width of about 200 nm. The morphology of **P-Co-5** and **P-20** were drastically changed to short nanorods (see Supporting Information for **P-Co-5**). Interestingly, at large dilution, samples (**P-50** and **P-100**) were found as hollow materials. The sizes of the nanomaterials of **P-Co-5** to **P-100** were very small, and good pictures were not obtainable from SEM. Additionally, SEM images of the materials do not give information about the interior of the materials and so these materials were subjected to TEM analysis. High resolution (300 KV) TEM images of the nanomaterials are shown in Figure 4. The TEM image of the **PANI** contained exclusively nanofibers of 4–6 μm length with 200 nm widths (see Supporting Information), which matched very well with that of its SEM image (see Figure 3). **P-Co-5** and **P-20** samples were devoid of any long nanofibers, but showed the presence of short nanorods of 0.5–0.7 μm length with 80–120 nm diameter. In

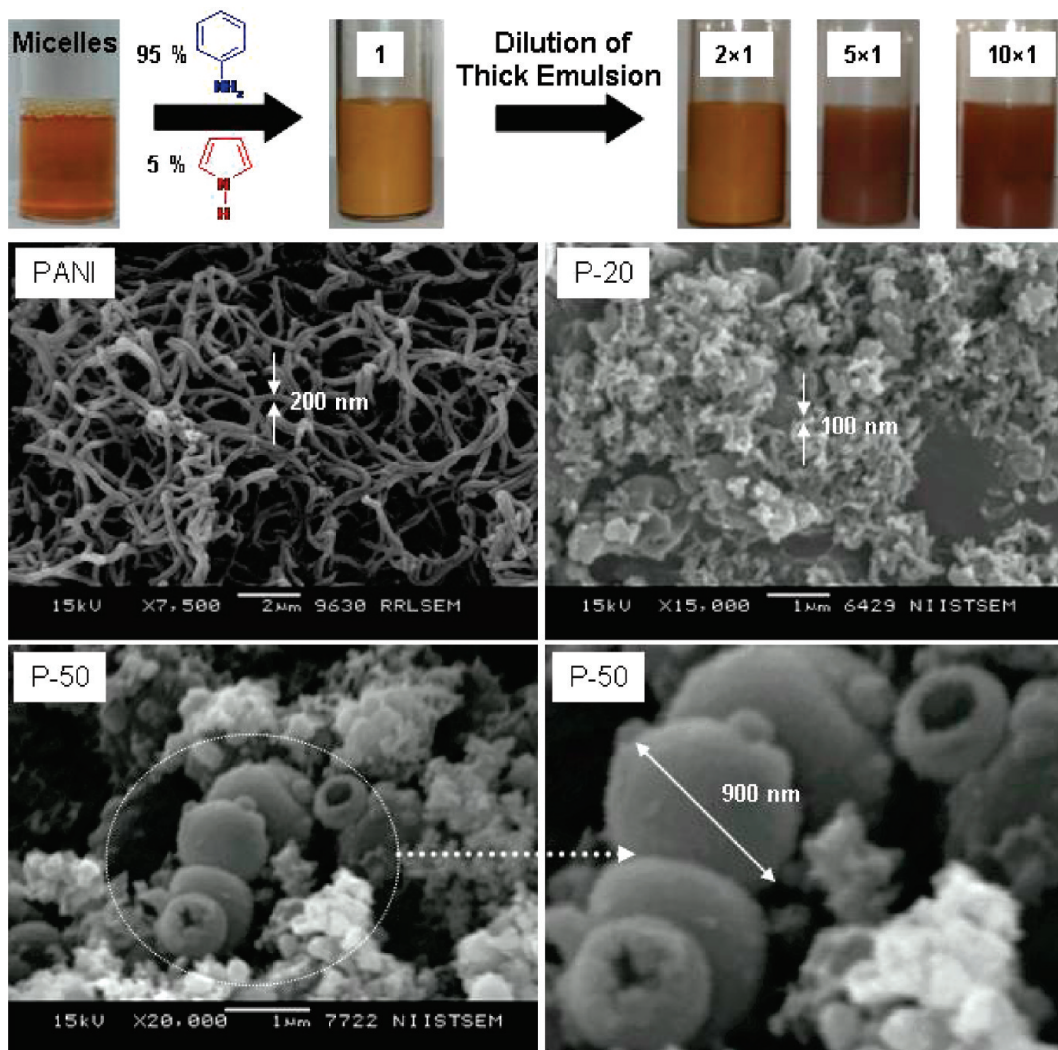


Figure 3. SEM images of PANI, P-20, and P-50. The vials contain the polymerization mixtures (surfactant + monomers in water) prior to APS oxidation.

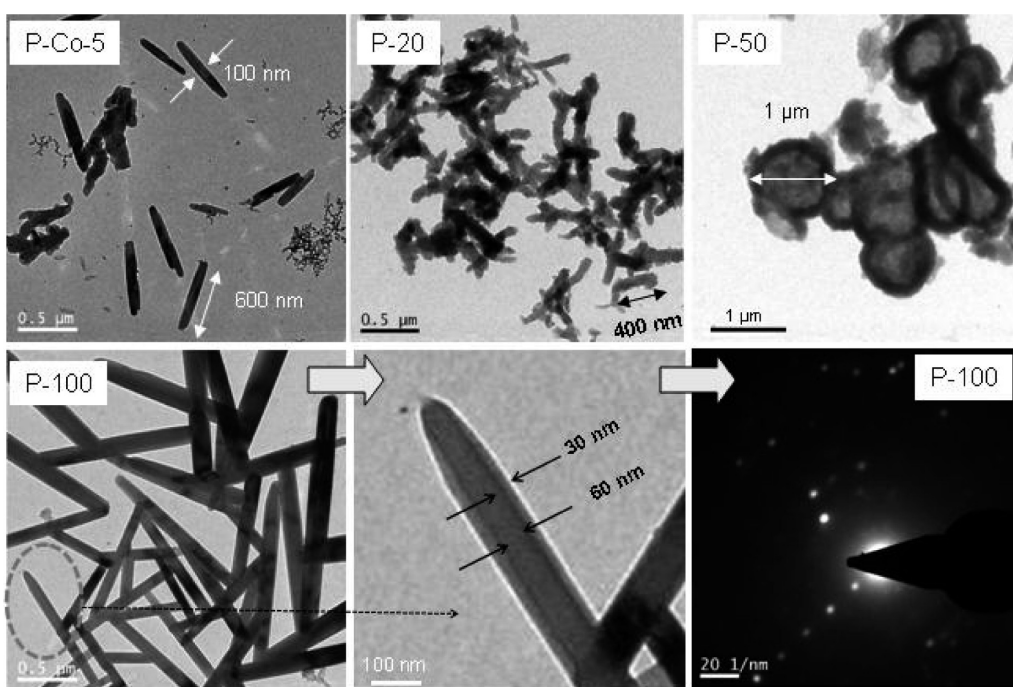


Figure 4. HR-TEM images of the P-Co-5, P-20, P-50, and P-100 and electron diffraction of P-100.

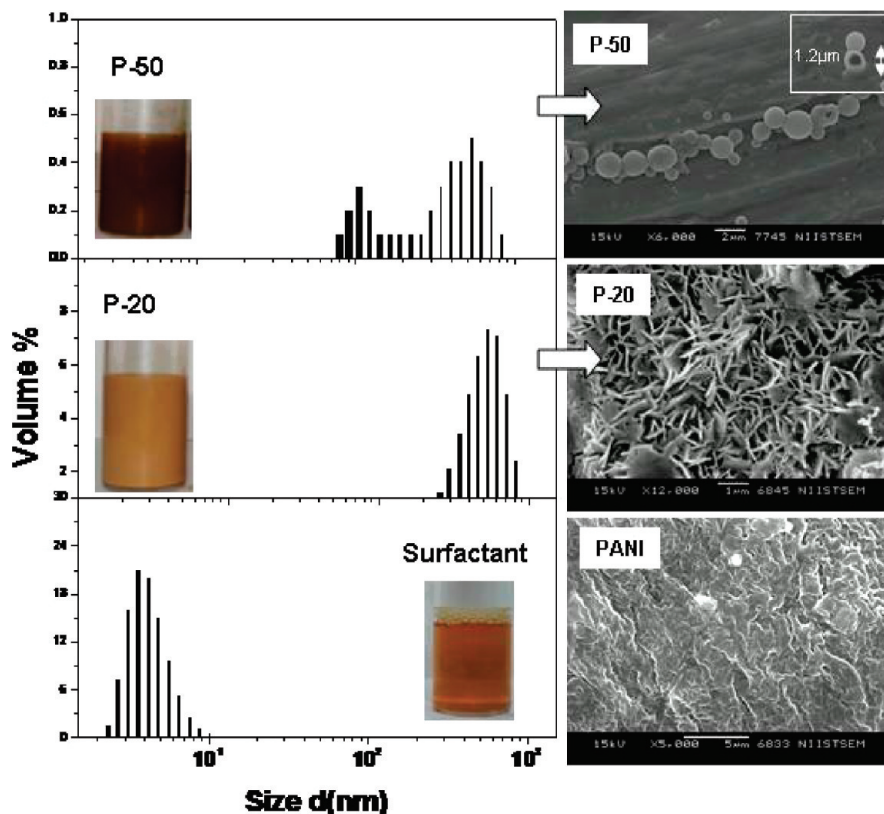


Figure 5. DLS histogram of surfactant, **P-20**, **P-50**, and SEM images of polymerization template of **PANI**, **P-20**, and **P-50**. The vials contain the polymerization mixtures (surfactant + monomers in water).

P-50, a large number of hollow spheres of 1 μm in diameter were found which was almost matching with the size and shape of its SEM image (see Figure 3). The wall thickness of the hollow sphere was obtained as ~ 80 nm. Interestingly, the largely diluted sample **P-100** exclusively showed nanotubes. The average wall thickness and the inner pore diameter of the nanotubes were obtained as ~ 30 and ~ 60 nm, respectively. The nanotubes were very short, and their length was varied from 1.2 to 1.8 μm . The nanotubes were further found to be highly crystalline and the electron diffraction pattern showed bright spots with periodicity corresponding to highly ordered layer-like structures in **P-100**.⁴¹ SEM and TEM of nanomaterials clearly gave evidence for the evolution of morphological transformation from long nanofibers to short nanorods and subsequently transferred into hollow spheres to highly crystalline nanotubes. The above morphological transformation was obtained in the present system by keeping all the reaction constituents and their composition the same, but by carefully varying their concentration by diluting the thick emulsion medium with water. It is very important to note that this is the first time such an evolution of nanomaterial morphologies were obtained in a single system without change in the polymerization process or composition of the constituents in the conducting polymer nanomaterials.

In the emulsion polymerization route, size and shape of the nanomaterials were highly dependent on their micellar state, and these micelles either in isolated or aggregated state determined the structures of the resultant nanomaterials. To study the mechanism of the evolution of nanomaterial transformation, the polymerization mixtures (emulsions) were subjected to dynamic light scattering (DLS, in solution) and electron microscopic analysis. The surfactant (1×10^{-3} M, above CMC) in water was subjected to DLS studies.^{30,31} DLS data revealed that azobenzenesulfonic acid surfactant molecule existed in the

form of the micelles of average diameter of 4.29 nm (see Figure 5). The orange or brown color emulsions shown in the vials (in Figures 3 and 5) are corresponding to the polymerization mixtures consisting of monomers + surfactant before the chemical oxidation by ammonium persulfate. The size of surfactant + aniline complex was obtained in the range of 3–5 μm .^{31c,d} DLS plots of the **P-Co-5** and **P-20** samples showed monomodal distribution with average micellar aggregates of ~ 500 nm (also see Supporting Information for **P-Co-5**). The DLS plots of **P-50** and **P-100** (see Figure 5 and also Supporting Information) showed bimodal distributions, with sizes in the micrometer range. DLS analysis clearly evidenced that the monomers + dopant existed as submicrometer size aggregates in the polymerization mixtures. The polymerization mixtures were very stable (for more than a week) which enabled us to trace the shape of the template aggregates by SEM shown in Figure 5. The polymerization mixtures were drop-cast on SEM stud and subjected to slow evaporation as reported earlier.^{31b} SEM image of the aniline + dopant template showed long fiberlike cylindrical-type aggregates template for polyaniline nanofibers.^{31b} SEM images of copolymer templates of **P-Co-5** and **P-20** were found as short flake-like aggregates, whereas the largely diluted polymerization mixtures **P-50** and **P-100** showed hollow-spherical aggregates. The hollow spherical morphology is a typical example for the formation of spherical vesicular template aggregates.^{30e} The short flake-like templates in **P-Co-5** and **P-20** produced short nanorods. Interestingly, in largely dilute cases **P-50** and **P-100**, the 3D spherical vesicular aggregates template for hollow spheres and nanotubes. Thus, the electron microscopic studies confirmed the evolution of nanofiber to nanorod to hollow sphere to nanotube is the resultant of the change in the shape of the polymerization templates from cylindrical to vesicular aggregates during the dilution process.

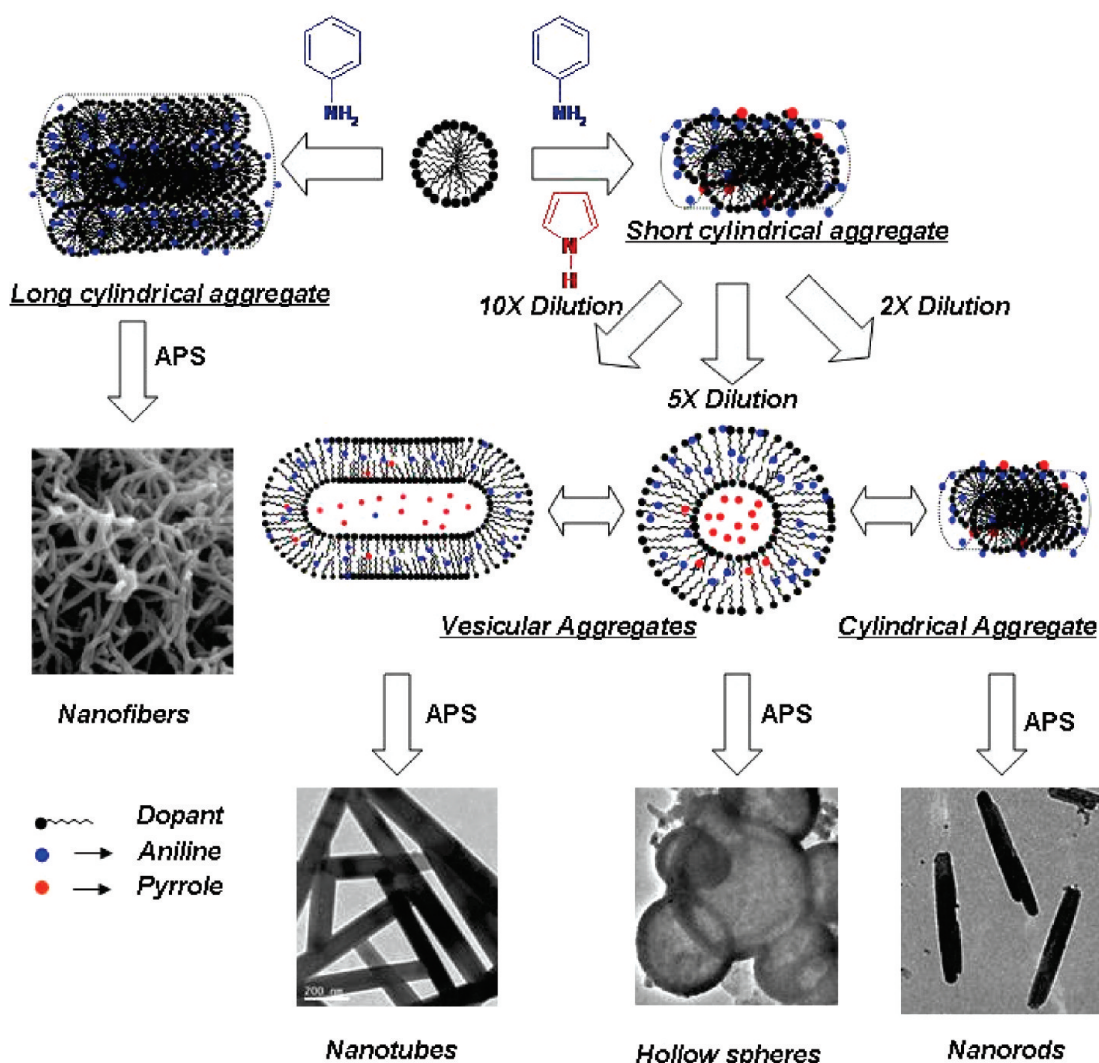


Figure 6. Plausible mechanism for the evolution of copolymer nanomaterials morphologies.

On the basis of the above studies, the following mechanism has been proposed for the evolution of nanomaterials morphology (see Figure 6). Amphiphilic azobenzene sulfonic acid forms micelles of size 4.3 nm in water. Dopant spherical micelles in the presence of aniline (aromatic primary amine) self-assemble as aggregated cylindrical micelles which produce nanofibers (PANI). Aniline monomer effectively neutralizes the polar head of the dopant in addition to their inclusion to the core of the micelles. In the presence of the comonomer pyrrole in feed (5 mol %), long-range cylindrical aggregates were truncated into short and thin cylindrical aggregates.^{31b} On subsequent dilution, the cylindrical assemblies were completely transformed to vesicular aggregates which account for the morphological evolution of nanorod to hallow sphere to nanotube. The various types of interactions of monomers (95% aniline + 5% pyrrole) with dopant during the dilution can be explained as follow: (i) aromatic monomer molecules interact with the dopant micelles in water to produce cylindrical aggregates, (ii) the subsequent dilution of cylindrical aggregates with addition of water (10 mL more) did not change the shape of the aggregates, and (iii) with excess dilution (more than 50 mL of water), the cylindrical aggregates transformed into spherical vesicular aggregates. The transformation of cylindrical to vesicular aggregates had been observed by Davies et al. in cetyl trimethylammonium bromide surfactant using aromatic molecules like 5-methylsalicylicacid as transformation agent.⁴² Recently, Anilkumar et al. from our

research group also reported such a cylindrical-to-vesicular transformation in a new amphiphilic 4-(3-dodecyl-8-enylphenoxy) butane sulfonic acid surfactant in dispersion route (water/toluene/aniline complex).^{30e} It supports the effect of dilution on the transformation of cylindrical aggregates into vesicular aggregates in the present system. To confirm the above hypothesis, the average sizes of the synthesized nanomaterials were compared with that of the polymerization templates based on their SEM and TEM images. The average diameter of a vesicular template aggregate was determined from the SEM image (see Figure 5) as $1.2 \pm 0.3 \mu\text{m}$. The average diameters of hollow spheres for the P-50 sample were obtained as 0.92 ± 0.2 and $1.00 \pm 0.1 \mu\text{m}$ based on SEM (see Figure 3) and TEM (see Figure 4), respectively. The diameter of vesicular template was almost identical to that of the synthesized hollow sphere which directly evidenced for the mechanism in Figure 6. The average length and diameter of the nanotubes were obtained as $1.6 \mu\text{m}$ and 120 nm , respectively, with a high aspect ratio of ~ 14 (length/width). If the transformation of hollow sphere to nanotube morphology would have occurred, then one would expect the circumference of hollow sphere ($2\pi r$) should be almost equal to $2L$, where L is the length of the tube (neglecting small contribution from both edges). This can be further easily understood by imagining the squeezing of filled spherical balloon into a long cylindrical one. The average circumference of the hollow sphere ($2\pi r$, $r = 0.5 \mu\text{m}$, from

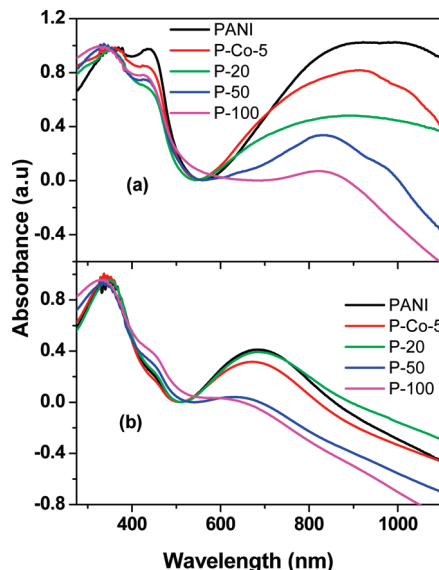


Figure 7. Absorption spectra of the **PANI**, **P-Co-5**, **P-20**, **P-50**, and **P-100** in doped state (a) and dedoped state (b).

TEM image) was calculated as $3.14 \mu\text{m}$ which was matching well with that of the twice the length of the nanotubes = $3.20 \mu\text{m}$ ($2L, L = 1.6 \mu\text{m}$ from TEM image). Hence, it proved that the nanotubes are nothing but the squeezed version of the hollow spheres. It confirmed that the hollow spheres and nanotubes were produced by the chemical oxidation of the vesicular aggregates formed by the dopant + monomers in the dilute polymerization route.

The amphiphilic nature and long alkyl tail of the renewable resource surfactant enhanced the solubility of the nanomaterials in water. The copolymer nanomaterials were freely dispersed in water by stirring under ultrasonication at room temperature. The UV-visible spectra of **PANI** and copolymers were recorded in their doped state (see in Figure 7). Polyaniline showed three transitions at 350, 430, and a broad peak at 850 nm with respect to $\Pi-\Pi^*$ transition, polaron to conducting band, valence band to polaron band, respectively.^{43,44} The UV-visible spectra of the **P-Co-5**, **P-20**, **P-50**, and **P-100** showed similar bands to that of **PANI**. The polaron bands were developed from the doping of the anionic surfactant molecule to the polyaniline matrix. Polaron band of **PANI** is highly delocalized compared to the **P-Co-5**, **P-20**, **P-50**, and **P-100**. As we employ more and more dilution the charge carrier bands are less delocalized. This result suggests that the pyrrole unit blocked the delocalization in the polymer chain backbone in the copolymers **P-Co-5**, **P-20**, **P-50**, and **P-100**. All the samples were dedoped using 1 M aqueous ammonia and their absorbance spectra were recorded (see Figure 7b). Upon dedoping the polaron band vanished from 800 nm, and quinoid band appears at 680 nm. Dedoped nanomaterials showed peaks at 360 and 650 nm, similar to conventional emeraldine base (EB) form.⁴⁵ The polymer nanomaterials were subjected to WXRD analysis to study the solid state ordering properties (see Figure 8). WXRD of polyaniline showed three peaks; two at higher angles at $2\theta = 25$ and 19.5 and one at lower angles at $2\theta = 6.75$.⁴⁶⁻⁴⁹ The lower angle peak arose from the long-range ordering of polyaniline chains via the doping of the surfactant molecules. The higher angle peaks were assigned to the aromatic chain-chain interaction in the polymers. **P-Co-5**, **P-20**, and **P-50** showed lower angle peaks at $2\theta = 3.6$ due to the long-range ordering from the lamellar arrangement of dopant molecules between the polymer chains.^{50,51} Interestingly in

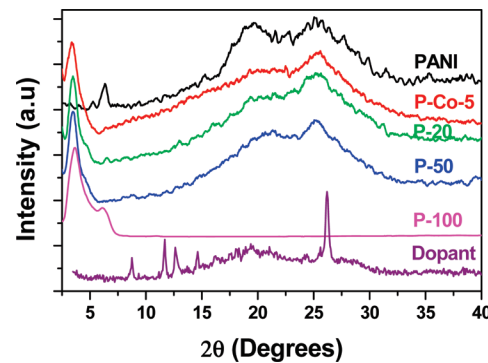


Figure 8. WXRD plots of the **PANI**, **P-Co-5**, **P-20**, **P-50**, **P-100**, and dopant.

P-100, the lower angle peaks were highly intense and sharp compared to other samples. The percentage crystallinities of the samples were determined from the WXRD patterns by comparing the area of amorphous domain with sharp crystalline peaks (see Table 2). The XRD patterns were deconvoluted computationally to calculate the integral intensities of amorphous and crystalline domains. The percent crystallinity of the samples **PANI**, **P-Co-5**, **P-20**, and **P-50** were almost identical in the range of 15–24%. The sample **P-100** showed a sharp low angle peak with complete vanishing of the amorphous domain ($2\theta = 15-30$), which resembled the typical nature of highly crystalline sample. The percent crystallinity of the **P-100** sample was obtained as more than 60%. The highly crystalline nature of **P-100** was further confirmed by the electron diffraction pattern from the HR-TEM of the nanotubes (see Figure 4). The electron diffraction patterns showed bright spots with regular periodicity corresponding to lamellar solid-state ordering. The reason for the highly crystalline nanotubes may be correlated to the slow kinetics of copolymerization of monomers at largely diluted polymerization samples (see Supporting Information). At higher dilution, the polymer chains have high tendency for the formation of long-range ordering via the lamella packing of surfactant chains.

Conductivity of the sample was recorded by four-probe conductivity techniques with PID controlled heating oven. All samples, **PANI**, **P-Co-5**, **P-50**, and **P-100**, were compressed into pellet and subject to $I-V$ measurements. All the samples showed a linear $I-V$ plot (see Figure 9a) and followed the ohm's behavior.⁵²⁻⁵⁴ The electrical resistance of the materials was obtained from slope of the $I-V$ plots at 30°C and their conductivities were reported in Table 2. The slopes of the $I-V$ plots of the samples (see Figure 9a) increase in the order of nanofiber < nanorod < hollow sphere < nanotube and indicate the increase in the resistance of the samples. The conductivity of the **PANI** was obtained in the range of 10^{-2} S/cm which was in accordance with that of the polyaniline doped with sulfonic acid derivatives.³⁰ The conductivities of nanorod, hollow sphere, and nanotubes were found one order lower than that of **PANI** nanofibers. To investigate the effect of temperature on the conductivity of the nanomaterials, they were subjected to variable temperature $I-V$ measurements from 30 to 100°C . Temperature dependent $I-V$ plot for **PANI** was shown in Figure 9b, and all other samples are in the Supporting Information. As expected with an increase in the temperature, the resistance decreases. The conductivity of the samples were determined from $I-V$ plots, plotted against temperature, and shown in Figure 10a. The **PANI** nanofiber showed much higher conductivity than other nanoforms. Since all the nanomaterials were synthesized using [monomers]/[dopant] = 75 (75 times lower

TABLE 2: Size, Shape, WXRD Data, and Conductivity of the Nanomaterials

sample	morphology ^a			WXRD			
	shape	length	width ^b (nm)	2θ (degrees)	d-spacing (Å)	crystallinity ^c (%)	σ^d (S/cm)
PANI	fiber	4 ± 0.5 nm	200 ± 20	6.4, 19.4, 25.1	13.8, 4.6, 3.5	15	1.2×10^{-2}
P-Co-5	rod	600 ± 50 nm	150 ± 10	3.3, 25.4	26.7, 3.5	24	4.2×10^{-3}
P-20	rod	425 ± 50 nm	90 ± 10	3.4, 25.3	25.9, 3.5	24	2.3×10^{-3}
P-50	hollow spheres		920 ± 100	3.6, 25.2	24.5, 3.5	24	2.1×10^{-3}
P-100	tubes	1600 ± 300 nm	120 ± 20	3.6, 6.1	24.5, 14.5	60	1.3×10^{-4}

^a The average nanodimensions of the material are calculated from the TEM images. ^b For hollow spheres the average diameter is given as width. ^c The percentage of crystallinity is calculated by comparing the area of amorphous and crystalline domain by deconvolution method. ^d The conductivity is measured using four-probe conductivity meter at 30 °C.

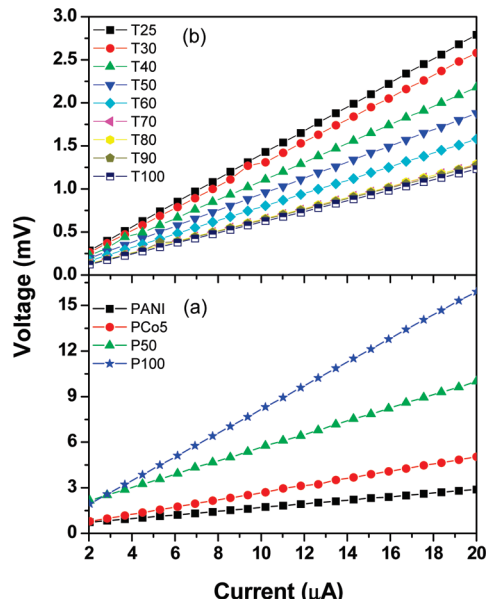


Figure 9. I – V plots of PANI, P-Co-5, P-50, and P-100 at room temperature (a). I – V plots of the PANI samples at different temperatures (b).

amount of dopant with respect to monomers), one may argue that these trends may be due to the difference in the doping level in the nanomaterials rather than the difference in their morphology. To rule out the difference in the doping level, all the sample pellets were dipped in 1 M HCl for 12 h for complete doping. The pellets were washed with water and methanol, dried in vacuum oven, and again subjected to variable temperature conductivity measurements (see Figure 10b). After HCl doping the conductivity of nanofiber, nanorods, and hollow spheres did not change much, whereas the nanotubes showed a slight increase in values. This detailed analysis revealed the difference in the conductivity of the samples arose from the difference in the morphology of the nanomaterials and not due to any other artifact such as incomplete doping, etc. To study the electronic transport behavior of the material, the resistance ($\ln R$) of the material was plotted over the temperature ($T^{-1/2}$) in the range of 298–373 K (see Supporting Information). In the insulating regime, the low-temperature resistivity $\rho(T)$ of the conducting polymer followed the exponential temperature dependence of variable range hopping (VRH): $\rho(T) = \rho_0 \exp(T_0/T)^m$, where the exponent $m = 1/2$ for the one-dimensional (1D) hopping process.^{53–56} T_0 is the Mott characteristic temperature and can be obtained from the slope of $\ln R$ vs $T^{-1/2}$ plot (see Supporting Information). The plots show a linear trend and follow the VRH model. The T_0 values for nanofiber, nanorods, hollow sphere, and nanotubes were obtained as 1.77×10^2 , 1.55×10^2 , 1.75×10^2 , and 1.8×10^2 K, respectively. These values were in accordance with earlier reports for metallic conductivity of

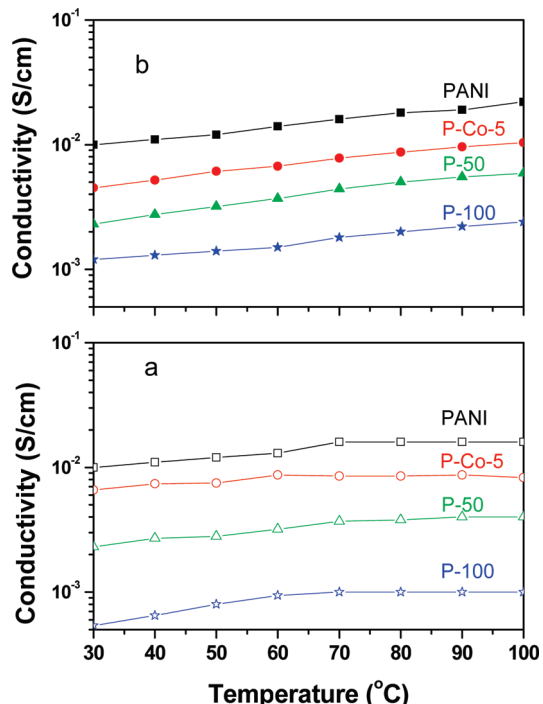


Figure 10. Conductivities of the nanomaterials: (a) actual and (b) after HCl doping.

polyaniline.^{54,55,50f} The comparison of the four-probe studies, morphology, solid state ordering and % crystallinity of the samples revealed that the conductivity of the nanomaterials were predominately controlled by the morphology. Since the composition of the all the nanoforms in the present investigation are almost identical, we can conclude that the polyaniline nanofibers are better conducting materials than other nanostructures. The empty voids occupied in the middle portion of the hollow sphere (also in nanotube) would restrict the conductivity of the electrons via the hopping process. Though the linear and thin geometry of nanotubes favored compactness in the solid state to form highly crystalline and ordered structures, a hollow inner domain behaved as an insulting layer resulting in poor conductivity. In brief, in the present investigation, we have successfully utilized the self-organized molecular templates for the evolution of multiple nanostructures without altering their chemical composition, which enabled us to correlate their conductivities, such as fibers, rods, hollow spheres, and nanotubes, in a single system.

Conclusion

We have developed a unique self-assembled molecular template approach for tracing the morphological evolution of conducting polymers exclusively in polyaniline-*co*-poly-

pyrrole nanomaterials. The important outcomes of the present investigation are as follows: (i) renewable resource amphiphilic azobenzenesulfonic acid dopant was developed to study the transformation of morphology such as nanofiber, nanorod, hollow sphere, and nanotube in a single system without change in the composition of their chemical constituents, (ii) the dopant micelles in water self-organized with aniline to produce thick emulsion consisting of cylindrical aggregates, which template exclusively for the polyaniline nanofibers, (iii) the self-organization of dopant micelles with aniline + pyrrole (95 + 5 mol %, respectively) produce short cylindrical aggregates and upon chemical oxidation these aggregates produce short nanorods, (iv) the dilution of the emulsion templates with known quantity of water resulted in the transformation of cylindrical to vesicular aggregates without phase separation, which template for hollow spheres and nanotubes, (v) the mechanistic aspects of the dilute polymerization route was studied by dynamic light scattering, which support the formation of micrometer-sized cylindrical and vesicular aggregates, (vi) the shape of the templates such as cylindrical and vesicular aggregates were confirmed by SEM and HR-TEM, (vii) the size and shape of the template aggregates matched very well with that of the resultant nanomaterials and confirmed the template-assisted polymerization mechanism, (viii) the structure and electronic properties of the nanomaterials were confirmed by NMR, FT-IR, and absorption spectroscopy, (ix) WXRD analysis revealed that the nanotubes produced at large dilution condition was found to possess more than 60% of crystallinity compared to that of the nanofibers, nanorods, and hollow spheres, (x) electron diffraction from the HR-TEM reveled the layerlike ordering in the nanotubes, (xi) the variable temperature four-probe conductivity measurements revealed that the samples showed typical $I-V$ plots, and (xii) the conductivity of the nanofibers were found higher at all the temperatures compared to that of all other nanoforms such as nanorod, hollow sphere, and nanotubes. The present investigation enabled us to establish the correlation between the morphology of the conducting polymer nanomaterials and their solid state ordering conductivity without disturbing either the compositions of the reactants or polymerization procedures. These new nanostructures are potential candidates for applications in electronic and electrical devices.

Acknowledgment. We thank the Department of Science of Technology, New Delhi, India, under the NSTI Programme-SR/S5/NM-06/2007 and SR-NM/NS-42/2009 for financial support. The authors thank Dr. Peter Koshy, Mr. M. R. Chandran, Dr. V. S. Prasad, Dr. U. Syamaprasad, and Mr. P. Guruswamy for SEM, TEM, and WXRD analysis. M. Jinish Antony thanks UGC-New Delhi, India, for Senior Research Fellowship (SRF).

Supporting Information Available: Synthesis characterization of the surfactant; NMR spectra **P-10**, **P-20**, **P-50**; FT-IR spectra of the nanomaterials; TGA of copolymers; SEM and TEM image of **P-Co-5**, **PANI**, respectively; DLS histograms of copolymer; $I-V$ plots for copolymers **P-Co-5**, **P-50**, **P-100**; $\ln R$ versus temperature $T^{-1/2}$ plot of the nanomaterial; photographs of the vials showing polymerization at different time intervals. This material is available free of charge via the Internet at <http://pubs.acs.org>.

References and Notes

- (1) Wallace, G. G.; Kane-Maguire, L. A. P. *Adv. Mater.* **2002**, *14*, 953.
- (2) Berdichevsky, Y.; Lo, Y. *Adv. Mater.* **2006**, *18*, 122.
- (3) Otero, T. F.; Cortes, M. T. *Adv. Mater.* **2003**, *15*, 279.
- (4) Wang, J.; Jiang, M. *Langmuir* **2000**, *16*, 2269.
- (5) Huang, J.; Virji, S.; Weiller, B. H.; Kaner, R. B. *J. Am. Chem. Soc.* **2003**, *125*, 314.
- (6) Huang, J.; Virji, S.; Weiller, B. H.; Kaner, R. B. *Chem.-Eur. J.* **2004**, *10*, 1314.
- (7) Bidon, G.; Billion, M.; Livache, T.; Mathis, G.; Roget, A.; Torres-Rodriguez, M. *Synth. Met.* **1999**, *102*, 1363.
- (8) Girotto, E. M.; De Paoli, M. *Adv. Mater.* **1998**, *10*, 790.
- (9) Korri-Yousoufi, H.; Srivastava, P.; Godillot, P.; Yassar, A. *J. Am. Chem. Soc.* **1997**, *119*, 7388.
- (10) Ramanathan, K.; Bangar, M. A.; Yun, M.; Chen, W.; Myung, N. V.; Mulchandani, A. *J. Am. Chem. Soc.* **2005**, *127*, 496.
- (11) Lee, J.-H.; Serna, F.; Schmidt, C. E. *Langmuir* **2006**, *22*, 9819.
- (12) Geetha, G.; Rao, C. R. K.; Vijayan, M.; Trivedi, D. C. *Anal. Chim. Acta* **2006**, *568*, 119.
- (13) (a) Wu, A.; Kolla, H.; Manohar, S. K. *Macromolecules* **2005**, *38*, 7873. (b) Li, X.-G.; Li, A.; Huang, M.-R. *Chem.-Eur. J.* **2008**, *14*, 10309–10317. (c) Li, X.-G.; Li, J.; Huang, M.-R. *Chem.-Eur. J.* **2009**, *15*, 6446–6455.
- (14) Jang, J.; Oh, J. H.; Stucky, G. D. *Angew. Chem., Int. Ed.* **2002**, *41*, 4016.
- (15) Zhong, W.; Liu, S.; Chen, X.; Wang, Y.; Yang, W. *Macromolecules* **2006**, *39*, 3224.
- (16) Zhang, X.; Manohar, S. K. *Chem. Commun.* **2004**, 2360.
- (17) Li, D.; Huang, J.; Kaner, R. B. *Acc. Chem. Res.* **2009**, *42*, 135.
- (18) De Armitt, C.; Armes, S. P. *Langmuir* **1993**, *9*, 652.
- (19) Shen, Y.; Wan, M. *Synth. Met.* **1998**, *96*, 127.
- (20) Haung, K.; Wan, M.; Long, Y.; Chen, Z.; Wei, Y. *Synth. Met.* **2005**, *155*, 495.
- (21) Bay, L.; Mogensen, N.; Skaarup, S.; Sommer-Larsen, P.; Jorgenson, M.; West, K. *Macromolecules* **2002**, *35*, 9345.
- (22) Liu, L.; Zhao, C.; Zhao, Y.; Jia, N.; Zhuo, Q.; Yan, M.; Jiang, Z. *Eur. Polym. J.* **2005**, *41*, 2117.
- (23) Zhou, C.; Han, J.; Song, G.; Guo, R. *J. Polym. Sci., Polym. Chem.* **2008**, *46*, 3563.
- (24) (a) Sari, M.; Talu, M. *Synth. Met.* **1998**, *94*, 221–227. (b) Fuselba, F.; B'elanger, D. *J. Phys. Chem. B* **1999**, *103*, 9044.
- (25) Li, X.; Zhang, X.; Li, H. *J. Appl. Polym. Sci.* **2001**, *81*, 3002.
- (26) Stejskal, J.; Trchova, M.; Ananieva, I. R.; Janca, J.; Prokes, J.; Fedorov, S.; Sapurina, I. *Synth. Met.* **2004**, *146*, 29.
- (27) Lim, V. W. L.; Kang, E. T.; Neoh, K. G.; Ma, Z. H.; Tan, K. L. *Appl. Surf. Sci.* **2001**, *181*, 317.
- (28) Kim, J. W.; Cho, C. H.; Liu, F.; Choi, H. J.; Joo, J. *Synth. Met.* **2003**, *17*, 135.
- (29) (a) Cho, C. H.; Choi, H. J.; Kim, J. W.; Jhon, M. S. *J. Mater. Sci.* **2004**, *39*, 1883. (b) Li, X.-G.; Lu, Q.-F.; Huang, M.-R. *Small* **2008**, *4*, 1201–1209. (c) Li, X.-G.; Wei, F.; Huang, M.-R.; Xie, Y.-B. *J. Phys. Chem. B* **2007**, *111*, 5829–5836.
- (30) (a) Anilkumar, P.; Jayakannan, M. *Langmuir* **2006**, *22*, 5952. (b) Anilkumar, P.; Jayakannan, M. *J. Phys. Chem. C* **2007**, *111*, 3591. (c) Anilkumar, P.; Jayakannan, M. *Macromolecules* **2007**, *40*, 7311. (d) Anilkumar, P.; Jayakannan, M. *Macromolecules* **2008**, *41*, 7706. (e) Anilkumar, P.; Jayakannan, M. *J. Phys. Chem. B* **2009**, *113*, 11614. (f) Anilkumar, P.; Jayakannan, M. *J. Phys. Chem. B*, published online November 19, 2009, <http://dx.doi.org/10.1021/jp909016r>. (g) Anilkumar, P.; Jayakannan, M. *J. Appl. Polym. Sci.* **2009**, *114*, 3531–3541.
- (31) (a) Antony, M. J.; Jayakannan, M. *J. Phys. Chem. B* **2007**, *111*, 12772. (b) Antony, M. J.; Jayakannan, M. *J. Polym. Sci., Part B: Polym. Phys.* **2009**, *47*, 830.
- (32) Mu, S.; Yang, Y. *J. Phys. Chem. B* **2008**, *112*, 11558.
- (33) Goto, H.; Akagi, K. *Macromolecules* **2002**, *35*, 2545.
- (34) Li, X. G.; Wang, L. X.; Zhu, Z. L.; Yang, Y. L. *J. Appl. Polym. Sci.* **2001**, *82*, 510.
- (35) Li, X. G.; Haung, M. R.; Wang, L. W.; Zhu, M. F.; Menner, A.; Springer, J. *Synth. Met.* **2001**, *123*, 435.
- (36) Li, X. G.; Chen, R. F.; Haung, M. R.; Zhu, M. F.; Chen, Q. *J. Polym. Sci., Polym. Chem.* **2004**, *42*, 2073.
- (37) Du, X.-S.; Zhou, C.-F.; Mai, Y.-W. *J. Phys. Chem. B* **2008**, *112*, 19836.
- (38) Omastova, M.; Trchova, M.; Kavarova, J.; Stejskal, J. *Synth. Met.* **2003**, *138*, 447.
- (39) Omastova, M.; Trchova, M.; Pionteck, J.; Prokes, J.; Stejskal, J. *Synth. Met.* **2004**, *143*, 153.
- (40) Zhang, X.; Zhang, J.; Song, W.; Liu, Z. *J. Phys. Chem. B* **2006**, *110*, 1158.
- (41) Jang, J.; Oh, J. H. *Chem. Commun.* **2002**, 2200.
- (42) Davies, T. S.; Ketner, A. M.; Raghavan, S. R. *J. Am. Chem. Soc.* **2006**, *128*, 6669.
- (43) Cabala, R.; Skarda, J.; Potje-Kamloth, K. *Phys. Chem. Chem. Phys.* **2002**, *2*, 3283.

- (44) Xia, Y.; Wiesinger, J. M.; MacDiarid, A. G. *Chem. Mater.* **1995**, *7*, 443.
- (45) Kang, E. T.; Neoh, K. G.; Tan, K. L. *Prog. Polym. Sci.* **1998**, *23*, 211.
- (46) (a) Jayakannan, M.; Annu, S.; Ramalekshmi, S. *J. Polym. Sci., Part B: Polym. Phys.* **2005**, *43*, 1321. (b) Jayakannan, M.; Anilkumar, P.; Sanju, A. *Eur. Polym. J.* **2006**, *42*, 2623–2631.
- (47) Dufour, B.; Rannou, P.; Fedorko, P.; Djurado, D.; Travers, J. P.; Pron, A. *Chem. Mater.* **2001**, *13*, 4032.
- (48) Laska, J.; Djurado, D.; Lunzy, W. *Eur. Polym. J.* **2002**, *38*, 947.
- (49) Jana, T.; Nandi, A. K. *Langmuir* **2000**, *16*, 3141.
- (50) Song, M. K.; Kim, Y. T.; Kim, B. S.; Kim, J.; Char, K.; Rhee, H. W. *Synth. Met.* **2004**, *141*, 315.
- (51) Wernet, W.; Monkenbusch, M.; Wegner, G. *Macromol. Rapid Commun.* **1984**, *5*, 157.
- (52) Long, Y.; Chen, Z.; Ma, Y.; Zhang, Z.; Jin, A.; Gu, C.; Zhang, L.; Wei, Z.; Wan, M. *Appl. Phys. Lett.* **2004**, *84*, 2205.
- (53) Long, Y.; Chen, Z.; Wang, N.; Ma, Y.; Zhang, Z.; Zhang, L.; Wan, M. *Appl. Phys. Lett.* **2003**, *83*, 1864.
- (54) Long, Y.; Chen, Z.; Zheng, P.; Wang, N.; Zhang, Z.; Wan, M. *J. Appl. Phys.* **2003**, *93*, 2962.
- (55) Long, Y.; Zhang, L.; Ma, Y.; Chen, Z.; Wang, N.; Zhang, Z.; Wan, M. *Macromol. Rapid Commun.* **2003**, *24*, 938.
- (56) Mativetsky, J. M.; Datars, W. R. *Phys. B*, **2002**, *324*, 191.

JP910636S